NANO LETTERS

pubs.acs.org/NanoLett

Letter

Competing Energy Scales in Topological Superconducting Heterostructures

Yunyi Zang, Felix Küster, Jibo Zhang, Defa Liu, Banabir Pal, Hakan Deniz, Paolo Sessi,* Matthew J. Gilbert,* and Stuart S.P. Parkin*

Cite This: *Nano Lett.* 2021, 21, 2758–2765

Read Online

ACCESS | Metrics & More | Article Recommendations | Supporting Information

ABSTRACT: Artificially engineered topological superconductivity has emerged as a viable route to create Majorana modes. In this context, proximity-induced superconductivity in materials with a sizable spin−orbit coupling has been intensively investigated in recent years. Although there is convincing evidence that superconductivity may indeed be induced, it has been difficult to elucidate its topological nature. Here, we engineer an artificial topological superconductor by progressively introducing superconductivity (Nb), strong spin−orbital coupling (Pt), and topological states (Bi_2Te_3). Through spectroscopic imaging of superconducting vortices within the bare *s*-wave superconducting Nb and within proximitized Pt and Bi_2Te_3 layers, we detect the emergence of a zero-bias peak that is directly linked to the presence of topological surface states. Our results are rationalized in terms of competing energy trends which are found to impose an upper limit to the size of the minigap separating Majorana and trivial modes, its size being ultimately linked to fundamental materials properties.

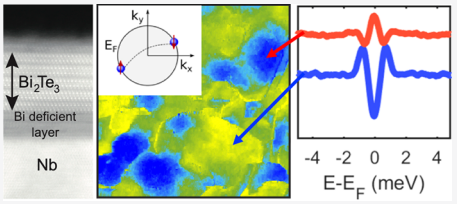

KEYWORDS: *Topological superconductors, heterostructures, Majorana modes, trivial modes*

INTRODUCTION

In the field of condensed matter physics, a Majorana Fermion (MF) is an emergent, fractionally charged quasiparticle that obeys non-Abelian exchange statistics[1,2] and is a key ingredient for topological quantum computation.[3] Generally speaking, MFs are expected to appear in the core of vortices in superconducting condensates with *p*-wave pairing symmetry.[4] A promising route to realize MFs relies on the creation of topological superconductor heterostructures where spin-split metallic states are proximitized with an *s*-wave superconductor (SC).[5−16] In this context, theoretical predictions suggest that the proximity effect between an ordinary *s*-wave superconductor and the Dirac surface states of a 3D time-reversal invariant topological insulator may lead to the emergence of MFs within vortices.[6] A similar realization scheme has been applied to ordinary electron systems characterized by strong spin−orbit coupling (SOC) and a large *g*-factor.[7,8] Under these circumstances, a spin nondegenerate 2D electron gas similar to the surface states of 3D topological insulators (TI) may be obtained by considering the combination of SOC and Zeeman effect. The SOC splits the spin degenerate band into a pair of spin nondegenerate bands while the Zeeman effect opens a gap at the crossing point of these two bands. When the chemical potential is tuned into this Zeeman gap, there is only one Fermi surface with helical spin polarization. A drawback of the above scheme is that the size of the Zeeman splitting must be larger than the size of the induced superconducting gap, a condition difficult to meet in ordinary 2D metals due to the orbital pair-breaking effect.

In the case of TIs, the Dirac, spin-split bands at the surface allows one to avoid the complications related to the presence of degenerate time-reversed pairs seen in strongly SOC systems. Proximity-induced superconductivity in prototypical 3D TIs such as Bi_2Se_3 and Bi_2Te_3 has been studied by scanning tunneling microscopy (STM), angle-resolved photoemission spectroscopy (ARPES), and quantum transport measurements, each of which reveal indirect yet tantalizing glimpses of the presence of MFs.[11,14−16] However, the topological insulator films used in the overwhelming majority of previous work are heavily electron doped, with a Fermi level lying well inside the bulk conduction bands. In such a scenario, topologically trivial and nontrivial states coexist, complicating the interpretation of the experimental results. Differences in the resultant manifestations of topological superconductivity that result from the physical properties inherent to different substrates are still not understood. For example, Cooper pairing in the Dirac surfaces states has been reported for Bi_2Se_3 grown on Nb[16] and for Bi_2Se_3 and Bi_2Te_3 on $NbSe_2$ substrates.[13,16] On the other hand, an absence of proximity-induced gaps has been reported for Bi_2Se_3 coupled to optimally doped cuprate superconductors,[17] a result in sharp contrast to fully gapped surface

Received: December 1, 2020
Revised: March 16, 2021
Published: April 1, 2021

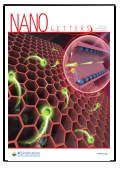

https://doi.org/10.1021/acs.nanolett.0c04648
Nano Lett. 2021, 21, 2758–2765

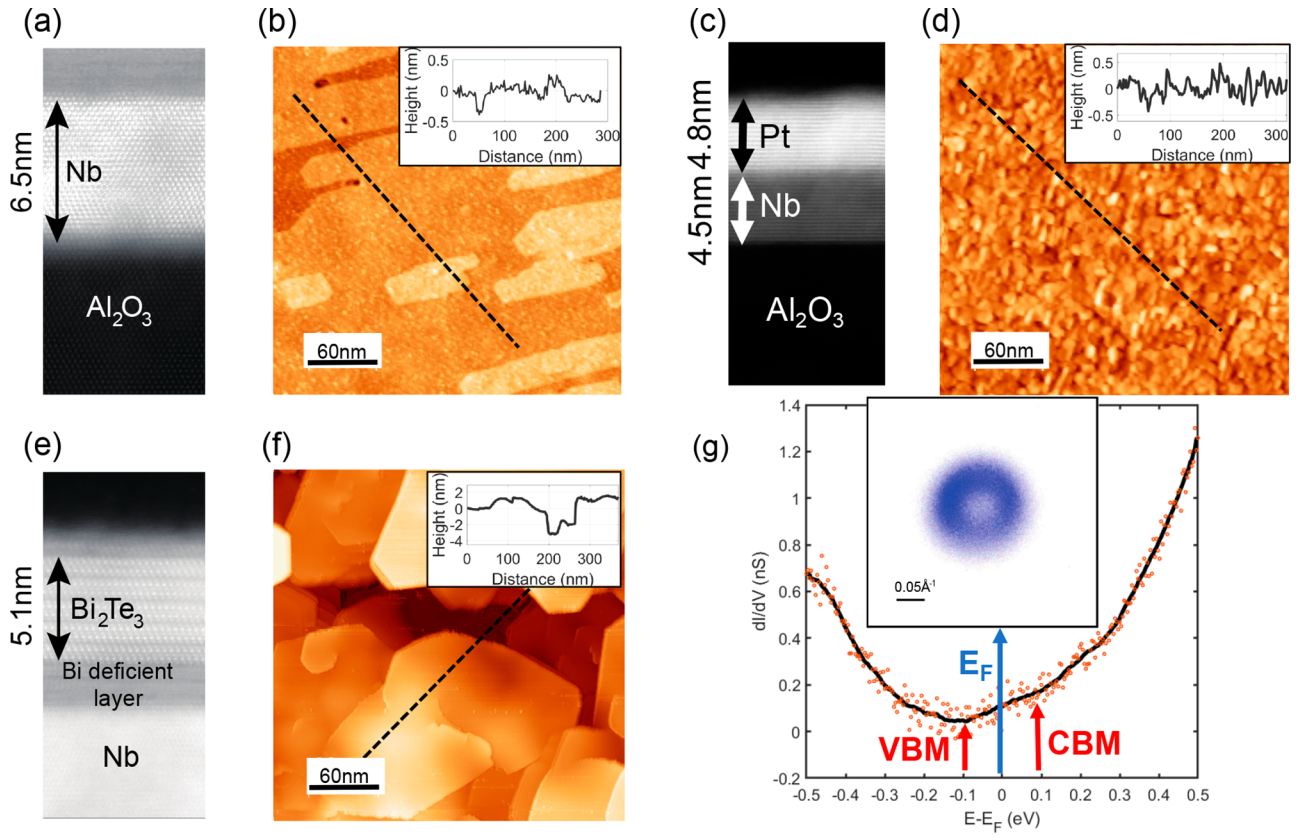

Figure 1. Heterostructures: (a, b) Nb/Al_2O_3, (c, d) $Pt/Nb/Al_2O_3$, and (e,f) $Bi_2Te_3/Nb/Al_2O_3$. For each heterostructure, the (a, c, e) and (b, d, f) panels report a STEM cross-sectional and STM surface image of the samples, respectively. (g) Spectroscopic characterization of the Bi_2Te_3 film. Both STS and ARPES data (inset) demonstrate that the Fermi level lies well inside the bulk gap, where only topological surface states exist. VBM and CBM refer to the valence band maximum and conduction band minimum, respectively.

states reported in an earlier study.[11] Several factors such as interface quality, superconducting penetration length, the presence of interface states, and interfacial lattice mismatch have been invoked to explain these different results.[17−21] More recently, the fabrication of bulk-insulating $(Bi_xSb_{1-x})_2Te_3/Nb$ heterostructures ($x = 0.62$) by flip-chip technique[10] resulted in the absence of proximity-induced superconductivity even for $(Bi_xSb_{1-x})_2Te_3$ films only two layers thick.[10] These results, compared to heavily doped Bi_2Se_3 films grown on the same substrate, suggested that the bulk states play a crucial role in transiting superconductivity to the topological Dirac states.[10]

Additionally, the unambiguous detection of MF signatures is severely complicated by the presence of Caroli-de-Gennes-Matricon (CdGM) states, low-energy excitations emerging within vortex cores of type-II superconductors which are characterized by a discrete energy spectrum with the lowest state emerging at about $E = \pm(1/2)\Delta^2/E_F$, with Δ being the superconducting energy gap and E_F the Fermi level.[22] Due to the very small value of Δ/E_F, CdGM states are generally detected as a symmetric peak in the local density of states centered at zero energy.[23] More recently, the discrete energy spectrum of CdGM states has been revealed in $FeTe_{0.55}Se_{0.45}$[24] and single layer $FeSe/SrTiO_3$.[25]

In this work, we examine the materials issues that are endemic to the observation of MFs in vortex cores of TIs by fabricating an artificial topological superconductor. Starting from superconducting Nb (110) films, we progressively introduce strong spin−orbit coupling and topological states by proximity with Pt and bulk-insulating Bi_2Te_3 films, respectively. By directly comparing the detailed spectroscopic characterization performed on all heterostructures, we reveal materials-dependent signatures through which MFs emerge only in the Bi_2Te_3 case. Backed up by theoretical simulations, our results provide compelling experimental evidence that the details of the underlying TI are not the impediment to the clear observation of topological superconductivity hosting Majorana modes but rather due to the existence of competing energy trends directly linked to fundamental materials properties and that set an upper limit to the maximum size of the induced minigap in the vortices.

RESULTS

Fabrication and Characterization of Topological Superconducting Heterostructures. Figure 1 illustrates the different heterostructures considered in this work. Figure 1a shows a cross-sectional scanning transmission electron microscopy (STEM) image of Nb films deposited on Al_2O_3 (see the Supporting Information for a description of sample preparation). The sharp interface and clear atomic resolution highlight the high crystalline quality of the Nb films. Figure 1b shows a topographic STM image acquired in the constant current mode. The surface consists of large terraces. The step height matches the distance between subsequent atomically flat planes along the Nb (110) crystallographic direction. This low surface roughness is crucial to promote a better epitaxy of the films subsequently grown on top of it.[26−28]

To create a superconducting condensate in a material characterized by strong SOC, a thin Pt film was directly

https://doi.org/10.1021/acs.nanolett.0c04648
Nano Lett. 2021, 21, 2758−2765

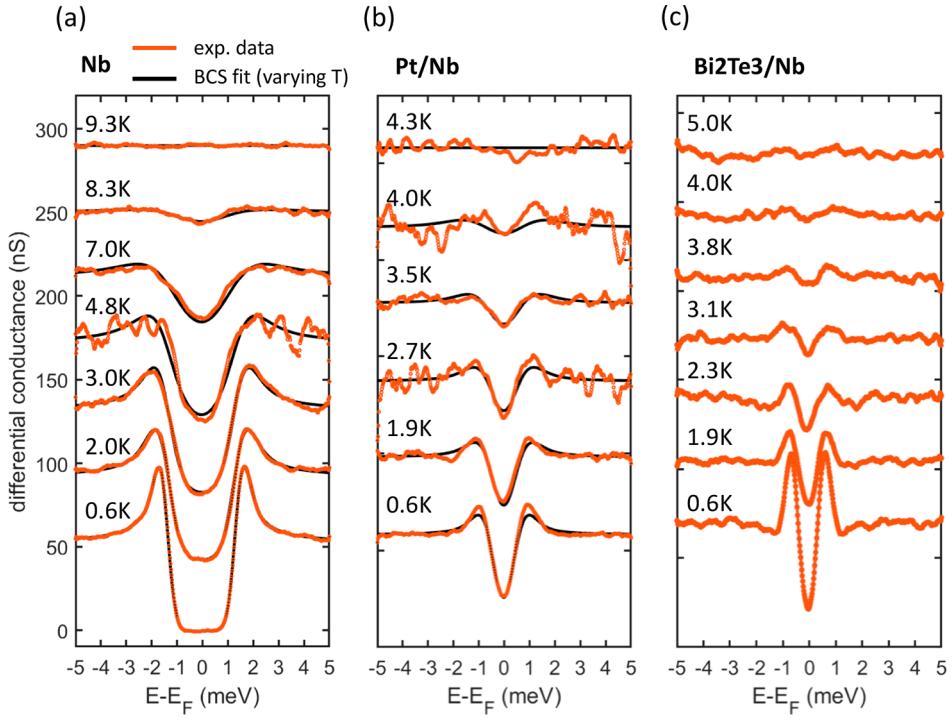

Figure 2. Temperature-dependent scanning tunneling spectroscopy. Superconducting energy gap observed in (a) Nb/Al_2O_3, (b) $Pt/Nb/Al_2O_3$, and (c) $Bi_2Te_3/Nb/Al_2O_3$ heterostructures at progressively higher temperatures. The experimental data (orange line) can be reproduced by a BCS fitting (black line) for Nb/Al_2O_3 and $Pt/Nb/Al_2O_3$. A strong deviation from this behavior is clearly visible for $Bi_2Te_3/Nb/Al_2O_3$.

deposited onto Nb to induce superconductivity via the proximity effect. A cross-sectional TEM image of the resulting heterostructure is reported in Figure 1c, demonstrating the creation of a sharp Pt−Nb interface, which is very important to allow Cooper pairs to efficiently tunnel into the Pt film.[29] The Pt layer grows along the (111) direction and has a thickness of 4.8 nm. The surface topography (Figure 1d) shows a homogeneous Pt film characterized by low surface roughness.

Finally, to scrutinize the effect of a topologically nontrivial band structure on proximity-induced superconductivity, thin films of the prototypical topological insulator Bi_2Te_3 were grown onto Nb underlayers. Contrary to previous reports where the unconventional superconductor BSCCO is used,[11] or where superconductivity and the charge density wave coexist such as in $NbSe_2$,[12−15] our Bi_2Te_3/Nb heterostructure represents the easiest possible platform for engineering topological superconductivity by directly coupling a TI to a conventional *s*-wave SC.[3−6] The thickness of our films amounts to five quintuple layers (QL) of the Bi_2Te_3 crystal structure, as discernible in Figure 1e.[30] A film with a thickness of 5 QLs maximizes the strength of the proximity effect while at the same time avoiding strong hybridization effects between the Dirac states hosted on its top and bottom surfaces.[31] The surface morphology visualized by STM consists of atomically flat terraces (Figure 1f). The line profile (inset of Figure 1f) reveals steps corresponding not only to the expected QL height but also to fractional-QL heights. As observed in earlier studies, this is a direct influence of the underlying substrate surface morphology, which imposes a vertical translation between two adjacent domains.[32] However, as described in the Supporting Information, this is found not to have any influence on the superconducting properties, which are homogeneous across the entire sample.

Being prototypical TI narrow gap semiconductors,[30] a precise spectroscopic characterization is crucial to precisely locate the Fermi level with respect to the bulk valence and conduction bands. Doping effects have been shown to shift the Fermi level well inside the bulk bands even for modest defect concentrations,[35,36] a scenario that is highly unfavorable for an unambiguous identification of topological effects. The scanning tunneling spectroscopy (STS) data shown in Figure 1g demonstrate that our Bi_2Te_3 films have a Fermi level residing inside the bulk gap.[37−39] This is further corroborated by the constant energy cut obtained by ARPES at room temperature (reported in the inset of Figure 1g), showing the typical isotropic shape of Dirac-like topological states and the absence of bulk bands. These observations make our TI/SC heterostructures ideal platforms to investigate topological superconductivity, since in sharp contrast to similar studies focusing on other prototypical TIs such as Bi_2Se_3 (heavily n-doped,[33,34]) or Sb_2Te_3 (heavily p-doped[35,36]), the absence of trivial states lying at the Fermi level allows the determination of the impact of material and interface quality as key ingredients required to engineer topological superconductivity.[3−6]

Superconducting Gaps Induced by the Proximity Effect. Figure 2 reports a series of differential conductance d*I*/d*U* spectra obtained at progressively higher temperatures on each of the systems investigated here, namely, superconducting Nb (Figure 2a), proximity-induced superconductivity in a strong spin−orbit coupled material Pt/Nb (Figure 2b), and proximity-induced superconductivity in a topologically nontrivial material, Bi_2Te_3/Nb (Figure 2c). A clear superconducting gap is visible in all systems at the lowest available temperature (600 mK). However, both quantitative as well as qualitative differences exist among the heterostructures. While Nb films show a superconducting transition temperature close

https://doi.org/10.1021/acs.nanolett.0c04648
Nano Lett. 2021, 21, 2758−2765

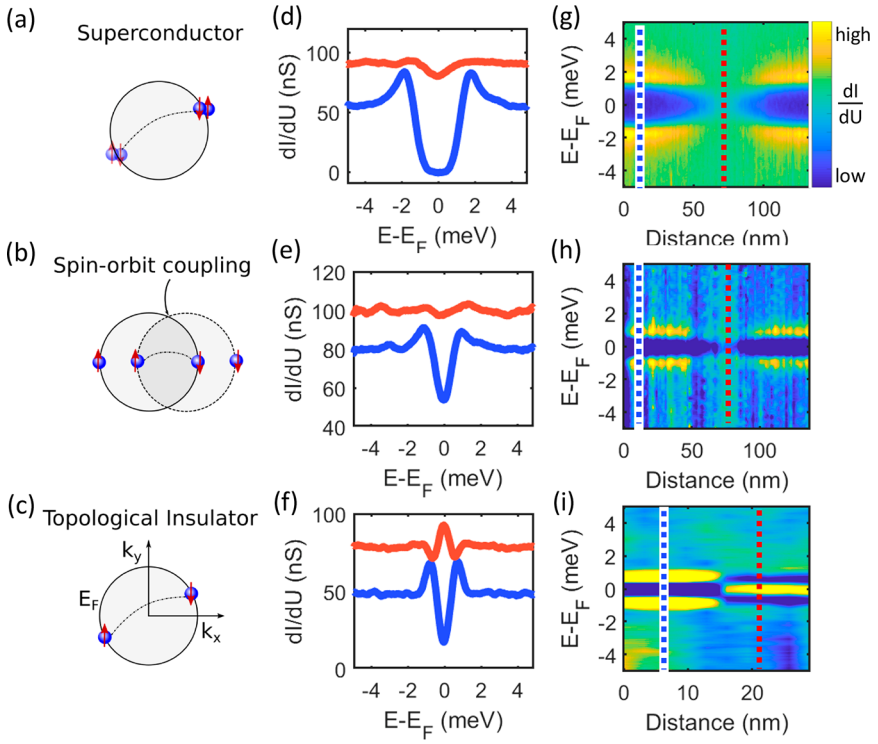

Figure 3. Spectroscopy across vortices. (a–c) Schematic illustration of superconducting pairing, (d–f) scanning tunneling spectroscopy data acquired by positioning the tip far away from the vortex (blue line) and at the vortex core (orange line), and (g–i) spectroscopic profile across a vortex taken for each heterostructure, along the white lines visible in the dI/dU maps in Figure S4. The data were acquired in a magnetic field of 200 mT applied perpendicular to the sample surface. For each heterostructure, the vertical lines visible in (g–i) correspond to the positions where the spectra reported in panels (d–f) have been acquired.

to 9 K, in agreement with bulk data,[40] a significantly lower temperature is necessary to create a superconducting condensate in Pt/Nb and Bi_2Te_3/Nb heterostructures. In both systems, superconductivity emerges only below 4 K, with the lower transition temperature being a direct consequence of superconductivity induced by the proximity effect. Additionally, while the Nb and Pt/Nb systems are both well fitted by an *s*-wave BCS-type spectral function,[41,42] this is not true for Bi_2Te_3/Nb. A strong deviation from standard *s*-wave BCS behavior is clearly signaled by the very sharp single-particle coherence peaks visible at the boundary of the excitation gap.[12,14] The use of the same underlayer (Nb) for both Pt and Bi_2Te_3 films, their similar thickness, and their same superconducting transition temperature set the foundation for a meaningful comparison in terms of their different electronic structures. To this point, we observe that the increased spin–orbit coupling in the Pt/Nb films produces a dI/dU spectrum that is closer in form to that of the linear dI/dU spectrum in Bi_2Te_3/Nb films, which possess the strongest spin–orbit coupling. Furthermore, the reduced Fermi velocity of Pt results in a smaller minigap leading to the observation of a smaller proximity-induced superconducting gap. In more general terms, our data serve to clearly highlight the decisive role played by the properties of the TI in the observation of phenomena pertaining to unconventional superconductivity under optimal conditions, i.e., the only states existing at the Fermi level in our Bi_2Te_3 films are those associated with the topological bands.

Spectroscopic Mapping of Vortices. The different Cooper pairing mechanisms among the heterostructures are schematically illustrated in Figure 3 a–c for Nb, Pt/Nb, and Bi_2Te_3/Nb, respectively. Without any significant spin–orbit coupling (Nb), the Fermi surface consists of two spin-degenerate energy bands. The pairing between electrons (indicated by the dashed line) can be described by the conventional BCS theory, and the resulting Cooper pairs are characterized by a standard *s*-wave singlet state. By introducing a heavy element thin film (Pt), the two spin bands are split in momentum space because of the combined action of spin–orbit coupling and lack of out-of-plane inversion symmetry naturally occurring at surfaces and interfaces, an effect known as the Rashba effect.[43,44] The introduction of SOC to the heterostructure opens the possibility of creating more complex and potentially unconventional superconducting phases. In particular, the presence of strong SOC and magnetic fields may effectively introduce a *p*-wave superconducting pairing ($p_x \pm ip_y$) in addition to the conventional *s*-wave, which is known to play a crucial role in the formation of topologically nontrivial superfluids hosting Majorana modes. However, since Fermion states still occur in degenerate time-reversed pairs in a Pt/Nb heterostructure, turning a spin-split 2D metal into a topological superconductor requires the introduction of Zeeman terms to imbalance the two *p*-wave degenerate components, resulting in an effective $p_x + ip_y$ superconductor. The degeneracy splitting induced by the magnetization must be larger than the size of the induced superconducting gap,[45−48] a condition difficult to meet in ordinary metals due to the orbital pair-breaking effect. As illustrated in Figure 3c, the odd number of spin-split bands hosted on the surface of topological insulators represent an ideal solution to induce topological superconductivity where Majorana Fermions are predicted to appear as zero-energy bound states in superconducting vortex cores.

https://doi.org/10.1021/acs.nanolett.0c04648
Nano Lett. 2021, 21, 2758−2765

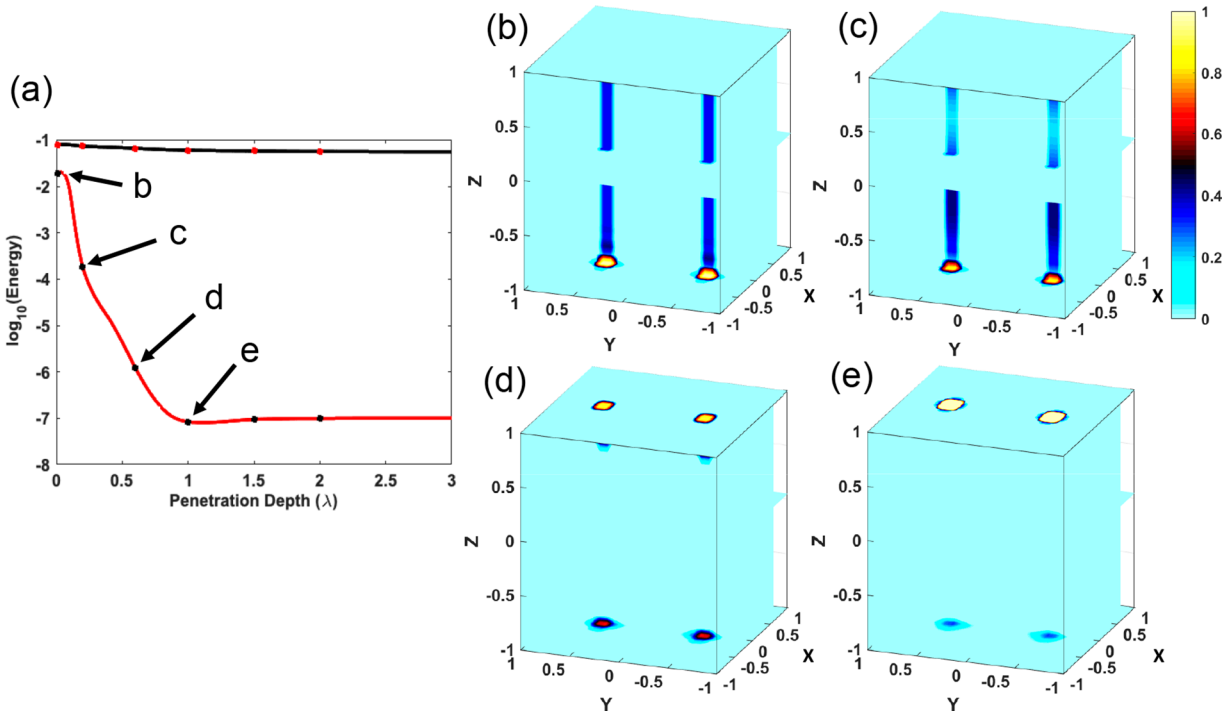

Figure 4. Probability distribution of lowest energy states in 3D. (a) Plot of the energy for the lowest and second lowest energy modes in the 3D system for $\lambda = 0.2$. We observe the formation of the topological phase in which the energy of the lowest lying state, the Majorana Fermion localized at the vortex core, approaches zero with increasing λ while the trivial second-lowest state remains constant in energy as the penetration depth is changed. The probability density distributions corresponding to penetrations depths of (b) $\lambda = 0.01a$, (c) $\lambda = 0.1a$, (d) $\lambda = 0.5a$, and (e) $\lambda = 1.0a$ showing the evolution of the states from being delocalized along the magnetic flux tube to localized in the vortex cores on the surface as the penetration depth of the superconductivity is increased.

The impact of the different electronic and spin-textures on the properties of the superconducting condensates has been experimentally probed by spectroscopic measurements acquired with magnetic fields applied perpendicular to the sample surface. In agreement with expectations for type-II superconductors, superconducting vortices appear in all heterostructures, i.e., Nb, Pt/Nb, and Bi_2Te_3/Nb, with the vortex density progressively increasing with increasing magnetic field strength in each case (see Figure S4 in the Supporting Information). However, unambiguous spectroscopic differences among the heterostructures are clearly revealed in Figure 3, with panels d, e, and f reporting STS spectra taken by positioning the tip in the vortex core (red lines) and far away from it (blue lines) for Nb, Pt/Nb, and Bi_2Te_3/Nb, respectively. While the superconducting gap vanishes at the vortex core in both Nb and Pt/Nb, a strong zero-bias peak emerges in the Bi_2Te_3/Nb case. A direct comparison of the data obtained on the three different heterostructures confirms the crucial role of the topological states, as opposed to simply strong SOC, in determining the properties of the Bi_2Te_3/Nb superconducting condensate. In particular, the zero-bias peak detected in the Bi_2Te_3/Nb case (see Figure 3 i) is consistent with the theoretically predicted signature of Majorana modes, which are expected to emerge in the vortex core of topological superconductors.[3−6] Additional experimental support for Majorana modes comes from the analysis of the spatial evolution of the spectroscopic properties in applied magnetic fields. Figure 3g−i report line spectra acquired across the superconducting vortices for Nb, Pt/Nb, and Bi_2Te_3/Nb, respectively (measured along the white lines visible in their respective dI/dU maps, see Figure S4). For Nb and Pt/Nb, the single-particle coherence peaks become progressively weaker while simultaneously converging into an X-shaped feature whose crossing point is located at the vortex core.[23] On the other hand, a sharp transition to a zero-bias peak is evidenced in the Bi_2Te_3/Nb case. In agreement with theoretical predictions for Majorana modes and in sharp contrast to the typical spatial behavior of CdGM states, the zero-bias peak does not split right off the vortex center, showing constant intensity over tens of nanometers.[15,49,50]

Modeling Topological Superconducting Heterostructures. To understand the physics contained within the vortex in proximity-coupled *s*-wave SC-3D time-reversal invariant topological insulator (STI) systems, we diagonalize a 3D TI Hamiltonian proximity coupled to an *s*-wave superconductor (see the Supporting Information for details). In our model, we consider two different cases of the penetration depth (λ) of the magnetic field, namely, the thin-flux limit and the thick-flux limit.[49] Specifically, the thin-flux limit occurs when the topological insulator layer is sufficiently thin and the magnetic flux that penetrates into the bottom layer of the topological insulator does not have sufficient distance to spread before reaching the top surface. Within the parameters that we have defined for the STI system, the thin-flux limit occurs when $\lambda \approx a$, with a being the lattice constant. In the thick-flux limit, which occurs when $\lambda \gg a$, the penetrating flux is dispersed uniformly within the TI film prior to reaching the top surface. Figure 4a reports the energies of the two lowest energy excitations emerging in the STI heterostructure as a function of the penetration depth λ, spanning from the thin-flux to the thick-flux regime. These states correspond to the Majorana Fermion (black line) and the first trivial bound state (red line),

https://doi.org/10.1021/acs.nanolett.0c04648
Nano Lett. 2021, 21, 2758−2765

which are both localized within the vortex core. While the energy of the Majorana Fermion approaches zero by progressively increasing λ, the topologically trivial state remains constant in energy as the penetration depth is changed. Their energy separation corresponds to the size of the minigap, which at first becomes larger by increasing λ and then stays constant as its maximum value reached $\lambda = 1$ (expressed in units of the lattice constant a). Figure 4b–e illustrate the spatial distribution of the lowest lying state in the STI heterostructure, corresponding to penetrations depths of (b) $\lambda = 0.01a$, (c) $\lambda = 0.1a$, (d) $\lambda = 0.5a$, and (e) $\lambda = 1.0a$. Within the thin-flux limit (panel b), the physics is dominated by wormhole Majorana states largely delocalized into the bulk such that they can tunnel through the vortex and hybridize, opening an energy gap which pushes them closer to the topologically trivial low state, as illustrated in Figure 4a. Figure 4c and d report the results obtained for λ values corresponding to the transition between the thin-flux and the thick-flux regimes, showing how Majorana states become progressively more localized onto the surface as the penetration depth is increased and reaching a scenario where the low energy mode is completely localized onto the surface for $\lambda = 1$ (panel). This regime corresponds to the best possible scenario for the detection of MFs in tunneling experiments, since it allows for the simultaneous maximization of both their spectral weight onto the surface as well as the size of the minigap which separates them from topologically trivial states.

DISCUSSION

The thick-flux condition is obviously fulfilled in our Bi_2Te_3/Nb samples, being that the thickness of the TI film (~5 nm) is much smaller than the Nb penetration depth (~40 nm[51]); this creates the best possible experimental conditions for the detection of Majorana modes. In our system, the zero-bias peak emerging inside vortices may be directly linked to the topological states, which are the only states present at the Fermi level in our bulk-insulating Bi_2Te_3 films. The spatial mapping is also consistent with theoretical predictions suggesting a local density of states distribution of Majorana modes that resembles a Y shape (see Figure 3i) which is qualitatively distinct from the typical V-shape of CdGM states.[23] However, the small energy gap separating MFs from CdGM states represents the major obstacle to energetically distinguish MFs from trivial states. Indeed, as evidenced by our model, the minigap size reaches a maximum which is directly related to fundamental material properties. With a proximity-induced SC gap of approximately 1 meV (see Figure 2 c) and a Fermi level located 150 meV above the Dirac point (see Figure 1 g), the minigap separating MFs from trivial states has a size of 0.01 meV. This value imposes severe experimental conditions to reach the quantum limit situation $T/Tc \ll \Delta/E_F$ which would allow the establishment of a direct relation between zero energy modes and MFs. A larger Δ/E_F value might be possible by either increasing the SC gap or by lowering the Fermi level. However, for a given class of materials, these values may not be independently changed, being directly linked to each other by competing and opposite energetic trends. For example, moving the Fermi level E_F closer to the Dirac point to increase the Δ/E_F ratio is intrinsically accompanied by a reduction of the proximity-induced superconducting energy gap Δ, with the smaller gap being a direct consequence of the lower density of states at the Fermi level. Being that these effects are intrinsically tied to one another, our results reveal that the size of the minigap, and consequently, the ability to energetically resolve MFs, is ultimately limited by fundamental and intertwined material properties.

CONCLUSION

The emergence of proximity-induced superconductivity in bulk-insulating Bi_2Te_3 demonstrates that topological Dirac states can be effectively driven into Cooper pairs. Our results provide compelling experimental evidence that the creation of a superconducting condensate onto the surface of a TI does not require the presence of bulk states,[10] but it does depend on the interface properties between materials, location of the Fermi energy, the induced superconducting gap, and the topological band structure. Our spectroscopic measurements reveal a strong deviation from a conventional BCS spectrum which can be directly linked to the presence of the topological states, as evidenced by the comparison with Nb and Pt/Nb cases. Additionally, we observe a zero-bias peak that emerges inside superconducting vortices in Bi_2Te_3/Nb heterostructures. The energy position and spatial distribution are found to be consistent with the expected signatures for Majorana modes.[15,50] Based on a detailed theoretical model, our results are rationalized in terms of the minigap separating MFs from CdGM states, revealing that the energy separation between states may be maximized by driving the system into the thick flux regime. However, the existence of competing energy trends provides an impediment to arbitrarily increasing its size beyond a maximum value dictated by fundamental materials properties. Overall, our results unveil the mechanisms by which are necessary to act to strengthen the proximity effects in TIs-Nb, evidencing the existence of inherent material limitations which underlie the unambiguous detection of Majorana modes in topological superconductors.

ASSOCIATED CONTENT

Supporting Information

The Supporting Information is available free of charge at https://pubs.acs.org/doi/10.1021/acs.nanolett.0c04648.

Growth parameters; reflection high-energy electron diffraction during growth; transmission electron microscopy characterization; spatial mapping of the superconducting gap; spatial mapping of the superconducting vortices; spectroscopy across vortices; spatial mapping of the superconducting vortices; and modeling topological superconducting heterostructures (PDF)

AUTHOR INFORMATION

Corresponding Authors

Paolo Sessi − *Max Planck Institute of Microstructure Physics, Halle 06120, Germany*; Email: paolo.sessi@mpi-halle.mpg.de

Matthew J. Gilbert − *University of Illinois at Urbana−Champaign, Department of Electrical and Computer Engineering, Urbana, Illinois 61820, United States*; Email: matthewg@illinois.edu

Stuart S.P. Parkin − *Max Planck Institute of Microstructure Physics, Halle 06120, Germany*; orcid.org/0000-0003-4702-6139; Email: stuart.parkin@mpi-halle.mpg.de

https://doi.org/10.1021/acs.nanolett.0c04648
Nano Lett. 2021, 21, 2758−2765

Authors

Yunyi Zang − *Max Planck Institute of Microstructure Physics, Halle 06120, Germany*

Felix Küster − *Max Planck Institute of Microstructure Physics, Halle 06120, Germany*

Jibo Zhang − *Max Planck Institute of Microstructure Physics, Halle 06120, Germany*

Defa Liu − *Max Planck Institute of Microstructure Physics, Halle 06120, Germany;* orcid.org/0000-0001-5199-6619

Banabir Pal − *Max Planck Institute of Microstructure Physics, Halle 06120, Germany*

Hakan Deniz − *Max Planck Institute of Microstructure Physics, Halle 06120, Germany*

Complete contact information is available at: https://pubs.acs.org/10.1021/acs.nanolett.0c04648

Notes

The authors declare no competing financial interest.

■ ACKNOWLEDGMENTS

The work in MPI-MSP was financially supported by the Deutsche Forschungsgemeinschaft (DFG, German Research Foundation) (project no. 314790414). M.J.G. acknowledges the financial support from the National Science Foundation (NSF) under grant no. DMR-1720633.

■ REFERENCES

(1) Majorana, E. Teoria simmetrica dell'elettrone e del positrone. *Nuovo Cimento* **1937**, *14*, 171.

(2) Wilczek, F. Majorana returns. *Nat. Phys.* **2009**, *5*, 614.

(3) Alicea, J. New directions in the pursuit of Majorana fermions in solid state systems. *Rep. Prog. Phys.* **2012**, *75*, 076501.

(4) Beenakker, C. Search for Majorana fermions in superconductors. *Annu. Rev. Condens. Matter Phys.* **2013**, *4*, 113.

(5) Sato, M.; Ando, Y. Topological superconductors: a review. *Rep. Prog. Phys.* **2017**, *80*, 076501.

(6) Fu, L.; Kane, C. L. Superconducting proximity effect and Majorana fermions at the surface of a topological insulator. *Phys. Rev. Lett.* **2008**, *100*, 096407.

(7) Sau, J. D.; et al. Generic new platform for topological quantum computation using semiconductor heterostructures. *Phys. Rev. Lett.* **2010**, *104*, 040502.

(8) Sau, J. D.; et al. Non-abelian quantum order in spin-orbit coupled semiconductors: search for topological Majorana particles in solid-state systems. *Phys. Rev. B: Condens. Matter Mater. Phys.* **2010**, *82*, 214509.

(9) Huang, C.; Zhou, B. T.; Zhang, H.; Yang, B.; Liu, R.; Wang, H.; Wan, Y.; Huang, K.; Liao, Z.; Zhang, E.; Liu, S.; Deng, Q.; Chen, Y.; Han, X.; Zou, J.; Lin, X.; Han, Z.; Wang, Y.; Law, K. T.; Xiu, F. Proximity-induced surface superconductivity in Dirac semimetal Cd_3As_2. *Nat. Commun.* **2019**, *10*, 2217.

(10) Hlevyack, J. A.; Najafzadeh, S.; Lin, M.-K.; Hashimoto, T.; Nagashima, T.; Tsuzuki, A.; Fukushima, A.; Bareille, C.; Bai, Y.; Chen, P.; Liu, R.-Y.; Li, Y.; Flötotto, D.; Avila, J.; Eckstein, J. N.; Shin, S.; Okazaki, K.; Chiang, T.-C. Massive suppression of proximity pairing in topological $(Bi_{1-x}Sb_x)_2Te_3$ films on niobium. *Phys. Rev. Lett.* **2020**, *124*, 236402.

(11) Wang, E.; Ding, H.; Fedorov, A. V.; Yao, W.; Li, Z.; Lv, Y.-F.; Zhao, K.; Zhang, L.-G.; Xu, Z.; Schneeloch, J.; Zhong, R.; Ji, S.-H.; Wang, L.; He, K.; Ma, X.; Gu, G.; Yao, H.; Xue, Q.-K.; Chen, X.; Zhou, S. Fully gapped topological surface states in Bi_2Se_3 films induced by a d-wave high temperature superconductor. *Nat. Phys.* **2013**, *9*, 621.

(12) Wang, M.-X.; Liu, C.; Xu, J.-P.; Yang, F.; Miao, L.; Yao, M.-Y.; Gao, C. L.; Shen, C.; Ma, X.; Chen, X.; Xu, Z.-A.; Liu, Y.; Zhang, S.-C.; Qian, D.; Jia, J.-F.; Xue, Q.-K. The coexistence of superconductivity and topological order in the Bi_2Se_3 thin films. *Science* **2012**, *336*, 52.

(13) Xu, S.-Y.; Alidoust, N.; Belopolski, I.; Richardella, A.; Liu, C.; Neupane, M.; Bian, G.; Huang, S.-H.; Sankar, R.; Fang, C.; Dellabetta, B.; Dai, W.; Li, Q.; Gilbert, M. J.; Chou, F.; Samarth, N.; Hasan, M. Z. Momentum-space imaging of Cooper pairing in a half-Dirac-gas topological superconductor. *Nat. Phys.* **2014**, *10*, 943.

(14) Xu, J.-P.; Liu, C.; Wang, M.-X.; Ge, J.; Liu, Z.-L.; Yang, X.; Chen, Y.; Liu, Y.; Xu, Z.-A.; Gao, C.-L.; Qian, D.; Zhang, F.-C.; Jia, J.-F. Artificial topological superconductor by the proximity effect. *Phys. Rev. Lett.* **2014**, *112*, 217001.

(15) Xu, J.-P.; Wang, M.-X.; Liu, Z. L.; Ge, J.-F.; Yang, X.; Liu, C.; Xu, Z. A.; Guan, D.; Gao, C. L.; Qian, D.; Liu, Y.; Wang, Q.-H.; Zhang, F.-C.; Xue, Q.-K.; Jia, J.-F. Experimental detection of a Majorana mode in the core of a magnetic vortex inside a topological insulator-superconductor $Bi_2Te_3/NbSe_2$ heterostructure. *Phys. Rev. Lett.* **2015**, *114*, 017001.

(16) Flötotto, D.; Ota, Y.; Bai, Y.; Zhang, C.; Okazaki, K.; Tsuzuki, A.; Hashimoto, T.; Eckstein, J. N.; Shin, S.; Chiang, T.-C. Superconducting pairing of topological surface states in bismuth selenide films on niobium. *Sci. Adv.* **2018**, *4*, No. eaar7214.

(17) Yilmaz, T.; Pletikosic, I.; Weber, A. P.; Sadowski, J. T.; Gu, G. D.; Caruso, A. N.; Sinkovic, B.; Valla, T. Absence of a proximity effect for a thin-films of a Bi_2Se_3 topological insulator grown on a top of a $Bi_2Sr_2CaCu_2O_{8+\delta}$ cuprate superconductor. *Phys. Rev. Lett.* **2014**, *113*, 067003.

(18) Xu, S.-Y.; Liu, C.; Richardella, A.; Belopolski, I.; Alidoust, N.; Neupane, M.; Bian, G.; Samarth, N.; Hasan, M. Z. Fermi-level electronic structure of a topological-insulator/cuprate-superconductor based heterostructure in the superconducting proximity effect regime. *Phys. Rev. B: Condens. Matter Mater. Phys.* **2014**, *90*, 085128.

(19) Li, W.-J.; Chao, S.-P.; Lee, T.-K. Theoretical study of large range proximity-induced s-wave-like pairing from a d-wave superconductor. *Phys. Rev. B: Condens. Matter Mater. Phys.* **2016**, *93*, 035140.

(20) Reeg, C. R.; Maslov, D. L. Hard gap in a normal layer coupled to a superconductor. *Phys. Rev. B: Condens. Matter Mater. Phys.* **2016**, *94*, 020501.

(21) Chiu, C.-K.; Cole, W. S.; Das Sarma, S. Induced spectral gap and pairing correlations from superconducting proximity effect. *Phys. Rev. B: Condens. Matter Mater. Phys.* **2016**, *94*, 125304.

(22) Caroli, C.; De Gennes, P.G.; Matricon, J. Bound Fermion state on a vortex line in a type II superconductor. *Phys. Lett.* **1964**, *9*, 307.

(23) Hess, H. F.; et al. Scanning-tunneling-microscope observation of the Abrikosov flux lattice and the density of stated near and inside a fluxoid. *Phys. Rev. Lett.* **1989**, *62*, 214.

(24) Chen, M.; Chen, X.; Yang, H.; Du, Z.; Zhu, X.; Wang, E.; Wen, H.-H. Discrete energy levels of Caroli-de-Gennes-Matricon states in quantum limit in $FeTe_{0.55}Se_{0.45}$. *Nat. Commun.* **2018**, *9*, 970.

(25) Chen, C.; et al. Observation of discrete conventional Caroli-de-Gennes-Matricon states in the vortex core of single layer FeSe/$SrTiO_3$. *Phys. Rev. Lett.* **2020**, *124*, 097001.

(26) Wildes, A.; Mayer, J.; Theis-Bröhl, K. The growth and structure of epitaxial niobium on sapphire. *Thin Solid Films* **2001**, *401*, 7.

(27) Kwo, J.; Hong, M.; Nakahara, S. Growth of rare-earth single crystals by molecular beam epitaxy: the epitaxial relationship between hcp rare earth and bcc niobium. *Appl. Phys. Lett.* **1986**, *49*, 319.

(28) Welander, P. B. Structural evolution of Re(0001) thin films grown on Nb(110) surfaces by molecular beam epitaxy. *J. Appl. Phys.* **2010**, *108*, 103508.

(29) Chang, W.; Albrecht, S. M.; Jespersen, T. S.; Kuemmeth, F.; Krogstrup, P.; Nygård, J.; Marcus, C. M. Hard gap in epitaxial semiconductor-superconductor nanowires. *Nat. Nanotechnol.* **2015**, *10*, 232.

(30) Zhang, H.; Liu, C.-X.; Qi, X.-L.; Dai, X.; Fang, Z.; Zhang, S.-C. Topological insulators in Bi_2Se_3, Bi_2Te_3 and Sb_2Te_3 with a single Dirac cone on the surface. *Nat. Phys.* **2009**, *5*, 438.

(31) Li, Y. Y.; et al. Intrinsic topological insulator Bi_2Te_3 thin films on Si and their thickness limit. *Adv. Mater.* **2010**, *22*, 4002.
(32) Borisova, S.; Kampmeier, J.; Luysberg, M.; Mussler, G.; Grützmacher, D. Domain formation due to surface steps in topological insulator Bi_2Te_3 thin films grown on Si(111) by molecular beam epitaxy. *Appl. Phys. Lett.* **2013**, *103*, 081902.
(33) Xia, Y.; Qian, D.; Hsieh, D.; Wray, L.; Pal, A.; Lin, H.; Bansil, A.; Grauer, D.; Hor, Y. S.; Cava, R. J.; Hasan, M. Z. Observation of a large-gap topological-insulator class with a single Dirac cone on the surface. *Nat. Phys.* **2009**, *5*, 398.
(34) Benia, H. M.; Lin, C.; Kern, K.; Ast, C. R. Reactive chemical doping of the Bi_2Se_3 topological insulator. *Phys. Rev. Lett.* **2011**, *107*, 177602.
(35) Hsieh, D.; Xia, Y.; Qian, D.; Wray, L.; Meier, F.; Dil, J. H.; Osterwalder, J.; Patthey, L.; Fedorov, A. V.; Lin, H.; Bansil, A.; Grauer, D.; Hor, Y. S.; Cava, R. J.; Hasan, M. Z. Observation of time-reversal-protected single-Dirac-cone topological-insulator states in Bi_2Te_3 and Sb_2Te_3. *Phys. Rev. Lett.* **2009**, *103*, 146401.
(36) Seibel, C.; Bentmann, H.; Braun, J.; Minár, J.; Maaß, H.; Sakamoto, K.; Arita, M.; Shimada, K.; Ebert, H.; Reinert, F. Connection of a topological surface state with the bulk continuum in Sb_2Te_3(0001). *Phys. Rev. Lett.* **2015**, *114*, 066802.
(37) Alpichshev, Z.; Analytis, J. G.; Chu, J.-H.; Fisher, I. R.; Chen, Y. L.; Shen, Z. X.; Fang, A.; Kapitulnik, A. STM imaging of electronic waves on the surface of Bi_2Te_3: topologically protected surface states and hexagonal warping effects. *Phys. Rev. Lett.* **2010**, *104*, 016401.
(38) Sessi, P.; Otrokov, M. M.; Bathon, T.; Vergniory, M. G.; Tsirkin, S. S.; Kokh, K. A.; Tereshchenko, O. E.; Chulkov, E. V.; Bode, M. Visualizing spin-dependent bulk scattering and breakdown of the linear dispersion relation in Bi_2Te_3. *Phys. Rev. B: Condens. Matter Mater. Phys.* **2013**, *88*, 161407.
(39) Chen, M.; Chen, X.; Yang, H.; Du, Z.; Wen, H.-H. Superconducting with twofold symmetry in $Bi_2Te_3/FeTe_{0.55}Se_{0.45}$. *Sci. Adv.* **2018**, *4*, No. eaat1084.
(40) Finnemore, D. K.; Stromberg, T. F.; Swenson, C. A. Superconducting properties of high-purity niobium. *Phys. Rev.* **1966**, *149*, 231.
(41) Bardeen, J.; Cooper, L. N.; Schrieffer, J. R. Theory of superconductivity. *Phys. Rev.* **1957**, *108*, 1175.
(42) Dynes, R. C.; Narayanamurti, V.; Garno, J. P. Direct measurements of quasiparticle-lifetime broadening in a strong-coupled superconductor. *Phys. Rev. Lett.* **1978**, *41*, 1509.
(43) Bihlmayer, B.; et al. Focus on the Rashba effect. *New J. Phys.* **2015**, *17*, 050202.
(44) Dal Corso, A. Clean Ir(111) and Pt(111) electronic surface states: a first-principle fully relativistic investigation. *Surf. Sci.* **2015**, *637*, 106.
(45) Oreg, Y.; et al. Helical liquids and Majorana bound states in quantum wires. *Phys. Rev. Lett.* **2010**, *105*, 177002.
(46) Alicea, J. Majorana fermions in a tunable semiconductor device. *Phys. Rev. B: Condens. Matter Mater. Phys.* **2010**, *81*, 125318.
(47) Potter, A. C.; Lee, P. A. Topological superconductivity and Majorana fermions in metallic surface states. *Phys. Rev. B: Condens. Matter Mater. Phys.* **2012**, *85*, 094516.
(48) Manna, S.; et al. Signature of a pair of Majorana zero modes in superconducting gold surface states. *Proc. Natl. Acad. Sci. U. S. A.* **2020**, *117*, 8775.
(49) Chiu, C.-K.; Gilbert, M. J.; Hughes, T. L. Vortex lines in topological insulator-superconductor heterostructures. *Phys. Rev. B: Condens. Matter Mater. Phys.* **2011**, *84*, 144507.
(50) Kawakami, T.; Hu, X. Evolution of the density of states and a spin-resolved checkboard-type pattern associated with the Majorana bound state. *Phys. Rev. Lett.* **2015**, *115*, 177001.
(51) Maxfield, B. W.; McLean, W. L. Superconducting penetration depth of niobium. *Phys. Rev.* **1965**, *139*, A1515.

https://doi.org/10.1021/acs.nanolett.0c04648
Nano Lett. 2021, 21, 2758−2765